© creative

Scientific paper

Modification of PVA Nanofiber by Simple Hot Water Treatment and Application on the Removal of Malachite Green Dye From Aqueous Solutions

Banaz A. Abdulghafar, Suhad A. Yasin and Nawzat S. Saadi²

¹ University of Duhok, College of Science, Department of Chemistry, Duhok City, Kurdistan Region, Iraq 42001

² University of Duhok, College of Science Department of Physics, Duhok City, Kurdistan Region, Iraq 42001

* Corresponding author: E-mail: banaz.abdulghafar@uod.ac suhad.yasin@uod.ac; nawzat@uod.ac

Received: 10-11-2023

Abstract

In this study, the crosslinking of PVA nanofiber was increased using solvent vapor treatment. Then, Fe_3O_4 nanoparticles were synthesized by a simple hot water technique and composited with the nanofiber. The study focuses on applying the modified PVA nanofibers to remove malachite green (MG) from water using different pH, contact times, and dye initial concentrations. The surface morphology of the nanofiber was determined using SEM, FTIR, and XRD techniques. SEM showed that the crosslinking was increased, and Fe_3O_4 nanoparticles appeared as agglomerates on the surface of the nanofiber. The removal percentages at optimal pH and contact time were 99.76%, and 99.5%, respectively. Thereafter, kinetics was studied by the linear pseudo-first order, pseudo-second order, Elovich equation, and Intraparticle diffusion models. Results demonstrated that the adsorption kinetics follow the pseudo-second order. Moreover, the adsorption isotherm was discussed using Langmuir and Freundlich equations. The Langmuir equation best described the adsorption with R^2 value of 0.9771, and the maximum removal was 128.205 mg/g. As a result, the MG dye molecules covered the PVA nanofiber/Fe₃O₄ nanoparticles in a monolayer and homogenous coverage. The results of this study are significant for industries' wastewater treatment as they provide a potential solution for the removal of MG dye from textile, paper, cosmetics, food, and aquaculture industries' wastewater.

Keywords: Iron oxide nanoparticles, modification of nanofibers, adsorption, malachite green, hot water treatment.

1. Introduction

Population growth and industrial development have resulted in water pollution, which is one of the most serious problems nowadays. Many types of pollutants may cause water pollution, but toxic organic pollutants have become a severe problem to the human environment and cause serious health issues due to their hazardous effects, chemical stability, and difficulty to remove.1 One type of these organic contaminators is water-soluble organic dyes that show extensive applications in industries like paints, textiles, plastic products, and so on. Organic dyes can change the color and properties of water even at low concentrations because of the existence of aromatic compounds and heavy metals in their structures.^{2,3} Also, they can reduce the transmission of light in aquatic systems, eventually decreasing the efficiency of the photosynthesis process of aquatic plants.^{4,5} In addition, the accumulation

of dyes in animals and plants can result in skin irritation, allergic dermatitis, mutations, and cancer, thus being harmful to the brain, kidneys, liver, central nervous system, and reproductive system in living organisms. Therefore, dyeing wastewaters are the riskiest wastewaters and are hard to purify.^{6,7} Moreover, malachite green (MG) dye, which is the chemical structure seen in Figure 1: (a), is a tri-phenyl methane cationic dye that has been widely employed in industries for dyeing purposes. On the other hand, oral consumption of MG is harmful due to the presence of nitrogen in its chemical structure and would be carcinogenic for both humans and animals. 8 Various physical, chemical, and biological techniques may be used for MG dye removal from wastewater, for instance, advanced oxidation processes, nanophotocatalysis, ceramic membrane separation, electrochemical techniques, and aerobic granular sludge.¹¹ Also, adsorption is widely used among these techniques and could be a predominant

method, since it's simple, economical, flexible, and easily implemented. The high efficiency of adsorption and the development of practical processes require the complete and fast adsorption of coloring materials by adsorbents. For that reason, chemical or physical modifications in adsorbents are beneficial to increase the kinetics and capacity of adsorption. In addition, the nanofiber's structural morphology has attracted considerable attention in various applications and fields. Electrospinning is a widely used technique to generate nanofibers with a broad range of characteristics and advantages. Porous webs of nanofibers with different sizes and shapes can result from this technique, which modifies and promotes the nanofiber's properties and applications. 12-14 For instance, porous structures have high specific surface area and can be used in oil clean up, and catalysis, grooved structures have surfaces with parallel lines and can be used in tissue engineering, 12 branched structures have large porosity, tiny diameters, excellent biological properties, and thermal insulation and can be utilized in air filtrations, energy storage and harvesting, photocatalysis, and oil cleanup.¹³ Also, crimped fibers that have spring-like behavior, notable surface area, and remarkable biological and piezoelectric properties are applied in tissue engineering, energy harvesting, wound dressing, drug delivery, and textile.14 One of these modifications is the use of nanoparticles to increase the process of adsorption. 15,16 In general, nanoparticles have attracted wide interest recently because of their high efficiency, low consumption of energy, large surface area, catalytic potential, and high reversibility.¹⁷ Specifically, iron nanoparticles have acquired massive scientific and technological attention as they have shown an outstanding capacity for the remediation of the environment.¹⁸ For example, iron nanoparticles have been utilized for the removal of chlorinated organic materials, 19-21 dyes, 22-24 heavy metals from water,²⁵ and nuclear contaminants degradation.²⁶ Furthermore, numerous ways have been applied for the synthesis of nanoparticles, such as gas condensation which was the first method to prepare nanoalloys and crystals, vacuum deposition, chemical precipitation, and electrodeposition.²⁷ Each of these methods may include many drawbacks like being specific to a few numbers of metals, being expensive, or requiring elevated temperatures that minimize their application. However, recently a simple process of using only hot water has been demonstrated as an alternative and novel method to produce iron nanoparticles. Unlike the previous methods, hot water treatment (HWT) can be applied to plentiful materials and requires depressed temperatures and low-cost equipment. It is catalyst-free, has a high yield of production, as well as is environment-friendly because it uses water as the main material that is non-toxic and safe to use.²⁸ In this study, polyvinyl alcohol (PVA) nanofiber, Figure 1: (b), was used as a membrane for the adsorption of MG dye in aqueous solutions after it was modified by two steps. Firstly, improving the mechanical properties, specifically increasing the crosslinking of the nanofiber through solvent vapor treatment (SVT). Secondly, synthesizing Fe₃O₄ nanoparticles from Fe metal powder by hot water treatment (HWT) and composite these nanoparticles to the previously crosslinked PVA nanofiber to ensure efficient dye isolation from water. Recent studies have shown that the mechanical strength of nanofiber mats can be enhanced by the solvent vapor technique without changing the dimension or the membrane morphology of the mats. Also, it is less aggressive for fiber welding. In this technique, nanofiber mats are exposed to solvent vapors at a particular temperature according to the solvent used, thus, the solvent vapor will facilitate fusion between fibers at their junction points and increase the crosslinking. In this instance, better adhesion between fibers can be achieved by utilizing solvents with high boiling points. Moreover, the crosslinking of the modified nanofibers will increase in a short time, and the porous structure of the alleged membranes can be controlled easily.²⁹⁻³³

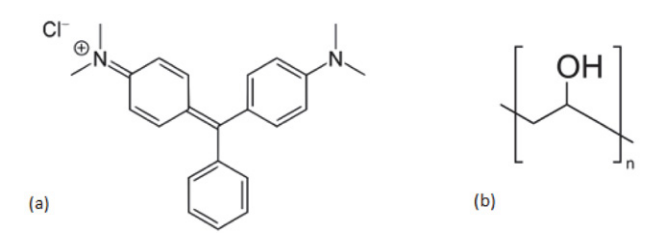


Figure 1: (a) chemical structure of malachite green (MG), (b) polyvinyl alcohol (PVA)

2. Materials and Methods

2. 1. Chemicals and Reagents

PVA nanofiber was purchased from Inovenso, N, N-Dimethylformamide (DMF), iron (Fe) powder, and Malachite green were from BDH Chemicals, NaOH from Sigma-Aldrich, and HCl was supplied by Ricca Chemical Company.

2. 2. Solvent Vapor Ttreatment (SVT)

Small coupons (approximately 9 cm \times 3 cm) of PVA nanofiber mats were prepared and placed on the top of a petri dish (D = 9 cm). DMF (3 mL) was used as a solvent and placed in a beaker sealed properly with the petri dish that contains the nanofiber coupon. The solvent was then evaporated on a hot plate stirrer at a temperature of 40 °C for 3 hours. After treatment, that sample was air dried for 24 hours to remove all solvent residual before further treatment.²⁹

2. 3. Hot Water Treatment (HWT)

At first, Fe metal powder was prepared for hot water treatment by removing native iron oxides that act as impurities and other organic contaminants using sanding paper polishing process. Then, the Fe powder was cleaned with acetone and deionized water (DI). The pre-washed Fe powder, along with the thermally treated PVA nanofiber membrane, was added to a glass beaker containing ultrapure DI water and then placed on the hot plate at a temperature of 75 °C for 1.5 hours with stirring. This temperature was selected as the standard temperature for water in this experiment, according to Nawzat. Saadi et al.²⁵ Also, one hour was defined as the critical time for the complete formation of Fe₃O₄ nanoparticles, but we increased the time to 90 min. At last, the composited nanofiber membrane was rinsed with DI water several times and air dried overnight, then delivered for SEM (Thermo Fisher Phenom Pro G6) and XRD (Bruker D8-Discover) to study the morphological, crystallographic, and chemical composition, respectively. On the other hand, Fourier transform infrared spectroscopy (FTIR) was performed for the water samples of the HWT as well as from the modified membrane for the study of the presence of Fe₃O₄ nanoparticles in both.

2. 4. MG Adsorption Studies

The batch operations of adsorption were studied for MG by taking the experimental conditions: pH, contact time, and effect of concentration. Firstly, the influence of pH was tested in the range (5.0–9.0) that was adjusted using 0.1 M NaOH and 0.1 M HCl solutions. A pH meter (JENWAY 3505) was also used for the measurements of the pH. The study of the pH effect was carried out using the adsorbent 0.003g and MG dye solution 5 ml of 10 mg/L concentration. The solutions were then stirred for 1 hour at room temperature. The MG absorbance was measured by using a UV-visible spectrophotometer (JANEWAY 7315) at 618 nm, which is the maximum absorbance wavelength of MG.³⁴ The ex-

periment of contact time for adsorption of MG was investigated, and the kinetic studies were performed at optimal circumstances: pH 8.0, adsorbent weight 0.003g, and 5 ml of MG solution 10 mg/L concentration. The batch tests were accomplished at room temperature with various time contacts (5, 10, 15, 20, 25, 30, 35, 40, 45, and 50) min.

Moreover, the impact of initial concentrations on MG adsorption was carried out by mixing and stirring 5 ml of different MG initial concentrations (10, 20, 30, 40, and 50) mg/L with pH 8 and 0.003 g of adsorbent for 20 minutes at room temperature until reached equilibrium.⁶

The following equation is used for calculating the (q_e) value, which is the equilibrium adsorption capacity and the removal percentage (R%) of MG.³⁵

$$q_e = \frac{(C_i - C_e) * V}{W} \tag{1}$$

$$R\% = \frac{c_i - c_e}{c_i} \times 100 \tag{2}$$

where; C_i = Initial concentration of MG (mg/L) C_e = equilibrium concentration of MG (mg/L) in the solution. V = Volume of dye solution (L) W = adsorbent mass (g).

3. Results and Discussion

3. 1. Characterization of PVA Nanofiber/ Fe₃O₄ Nanoparticles

3. 1. 1. SEM

In this study, the morphology of the modified PVA nanofiber before and after both treatments, SVT and HWT, was investigated by scanning electron microscopy (SEM). Figure 2: (a), shows the PVA mats before treatments, while, Figure 2: (b), represents the morphological and conformational changes that happened on the matt

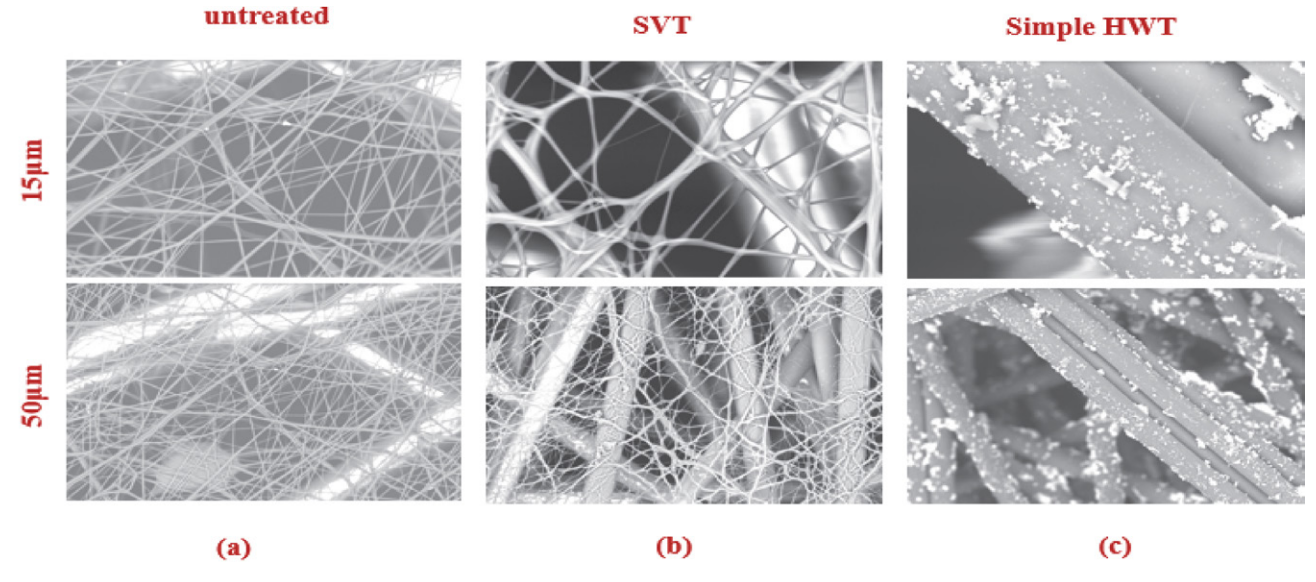


Figure 2: SEM of (a) untreated PVA nanofiber, (b) PVA nanofiber after SVT, (c) formation of PVA nanofiber/ Fe₃O₄ nanoparticles by HWT

after SVT when the mats were exposed to DMF vapor for 3 hours. It is obvious from the figures that in both 15µm and 50µm the crosslinking among the nanofibers has increased. Furthermore, a significant swelling has appeared on nanofibers, that may occur as a result of the absorbance of an amount of solvent vapor by nanofibers as there is an affinity of nanofibers to solvent. Also, Figure 2: (c), indicates the presence of iron oxide Fe₃O₄ nanoparticles on the PVA nanofiber surface that have irregular shapes that adsorb like aggregates on the nanofiber surface. The formation of different particle sizes may be a result of the agglomeration of nanoparticles on different sides of nanofiber during the sample preparation.³⁶ The mechanism by which Fe₃O₄ nanoparticles are present on the nanofiber's surface can be explained by a combination of the Fe₃O₄ nanoparticle's growth and deposition processes. In the first process, iron oxide ions can form on the Fe powder surface during HWT, release into the water, and then grow on the nanofiber, forming nanoparticles. This process, which is called plugging, is explained in more detail in the previous study.²⁵ In the deposition process, Fe₃O₄ nanoparticles grown on Fe metal powder can be detached from the powder surface and re-deposited on nanofibers.

3. 1. 2. Characterization of Fe₃O₄ Nanoparticles by (FTIR)

Fourier transform infrared spectroscopy (FTIR) gives information on nanoparticle structures from the

Fe₃O₄ nanoparticle's bond vibrational modes. Although it is incapable of quantifying the generated nanoparticles precisely in the samples, it provides a qualitative identification of the proportion of the produced nanoparticles. Figures 3 (a), and (b), show the infrared spectra of Fe₃O₄ nanoparticles presented in water samples after HWT and PVA nanofiber/Fe₃O₄ nanoparticles, respectively. To indicate the presence of Fe₃O₄ nanoparticles, the range of 800-400 cm⁻¹ was a characteristic of the Fe-O bond. In Figure 3: (a), Fe₃O₄ showed characteristic peaks at 469 cm⁻¹ and a maximum peak at 569 cm⁻¹ with a shoulder at 745 cm⁻¹ which was attributed to surface oxidation.³⁷⁻³⁹ Besides, Figure 3: (b), represents the formation of Fe₃O₄ on PVA nanofiber and shows additional peaks in the spectral range 501-575 cm⁻¹ with a broad spectrum at 723 cm⁻¹ while no peaks appeared around the 400 cm⁻¹ region. Moreover, the two peaks observed at 616 cm⁻¹ and 636 cm⁻¹ identify Fe_{Th}-O-Fe_{Oh} stretching vibrations on PVA nanofiber, where, Fe_{Th} is iron tetrahedral and Fe_{Oh} is iron octahedral. The appearance of the broadband at 3397 cm⁻¹ corresponded to the O-H group stretching vibrations, 2966 cm⁻¹ was the peak for the C-H bond, and the 1088 cm⁻¹ peak referred to the Fe-O-C bond.⁴⁰ The decrease in peak intensity in PVA nanofiber/Fe₃O₄ nanoparticles suggests the interaction between (C-H) and (O-H) groups of the nanofiber with Fe₃O₄ nanoparticles and indicates the well dispersion of the nanoparticles on the surface of the PVA nanofiber. 41

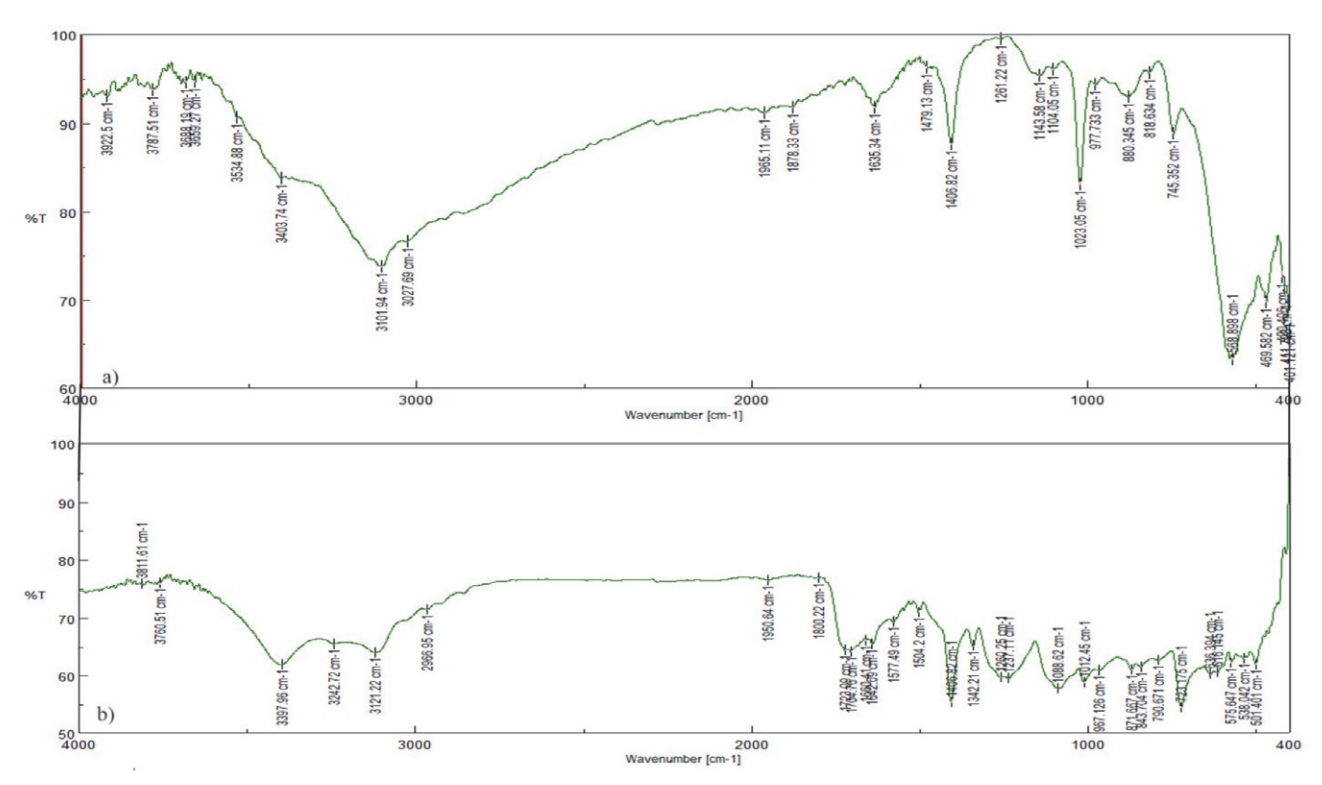


Figure 3: (a) FTIR spectrum of Fe_3O_4 nanoparticles in water samples synthesized by simple HWT, (b) FTIR spectrum of PVA nanofiber/ Fe_3O_4 nanoparticles synthesized by simple HWT

3.1.3 Characterization of Fe₃O₄ Nanoparticles by X-ray Diffraction (XRD)

The XRD charts of the $\mathrm{Fe_3O_4}$ nanoparticles and composite with PVA nanofiber were compared and shown in Figure 4. The spectra of XRD of the nanoparticles showed three diffraction peaks of 11.46, 15.85, and 149.15. Also, the XRD pattern of PVA nanofiber/ $\mathrm{Fe_3O_4}$ nanoparticles showed four peaks of 14.26, 54.10, 43.99, and 347.66. These peaks confirm the formation of $\mathrm{Fe_3O_4}$ nanoparticles in both samples as related to (JCPD98-026-3010). The two XRD spectra show two sharp peaks that appeared with 20 of 72.565 and 72.515, which are identical to those of reference and indicate the presence of $\mathrm{Fe_3O_4}$ nanoparticles. These data also detected that the nanoparticles have crystalline and spinel structures.

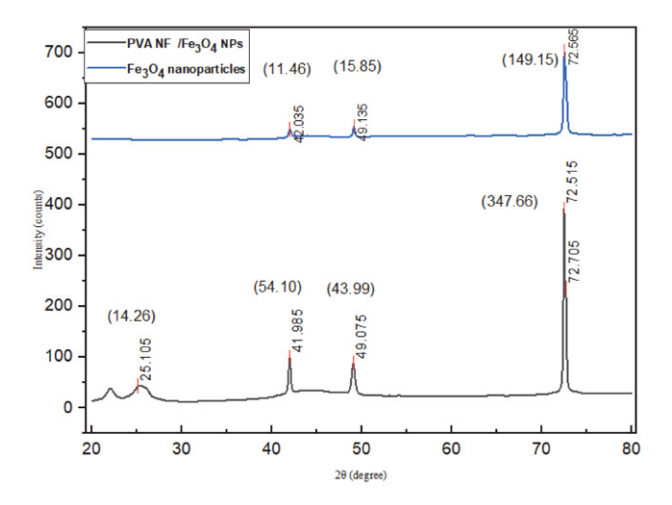


Figure 4: XRD diffraction of Fe_3O_4 nanoparticles compared to PVA nanofiber $/Fe_3O_4$ nanoparticles

3.2 Effect of pH

It is substantial to examine the impact of pH on the adsorption of MG because pH has an essential role in ad-

sorption capacity. It has an influence on the surface charge of the adsorbent, the tendency of the existent compounds in the solution to ionize, the adsorbent's active sites functional groups dissociation, and also the solution dye chemistry. 43 MG has p K_a of 10.3 which protonates under acidic conditions and deprotonates at higher pH values and a high positive charge is detected on the dye molecule at lower pH due to its protonation. 44,45 Also, it was perceived in this study that the adsorption is strongly dependent on pH and the superior adsorption was on pH 8 with a top removal rate of 99.76% which means that the electrostatic interactions between MG dve and the adsorbent are strong on this pH value that result in a high adsorption capacity. On the other hand, under acidic conditions low adsorption rates are observed and that is due to the excess availability and high concentrations of positive charge resulting from H⁺ protons and cationic dye molecules in the solution. Furthermore, the surface of the membrane may be positively charged, causing repulsions with the cationic dye molecules and decreasing the removal rates. The pH effect on the adsorption capacity of MG on PVA nanofiber/ Fe₃O₄ nanoparticles was examined over pH values (5.0, 6.0, 7.0, 8.0, and 9.0) using 0.1N NaOH, and 0.1N HCl solutions to adjust pH. Figure 5 explains the amount of removal of MG as a function of pH for the adsorbent initial concentration of 10 mg/L. The adsorption capacity was high at pH 8, but at lower pH values (4-7) the adsorption was low, and at pH 9 it decreased again.

3. 2. Effect of Contact Time

Figure 6 exhibits the time effect on the removal of the MG dye process. It's shown that the percentage of the removal of MG kept increasing with time until the maximum removal of color was seen at 20 min, with a maximum removal of 99.5%. The process of adsorption was fast from the beginning to 20 minutes when the removal of dye was achieved, which resulted from the attraction of charges on the adsorbent surface to MG dye. After that, the ad-

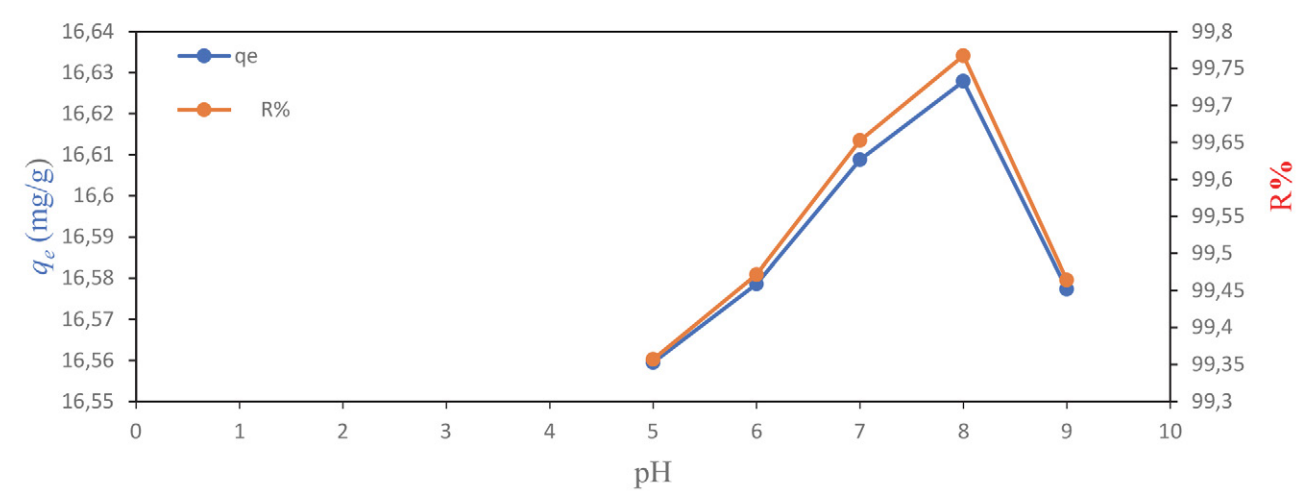


Figure 5: The effect of pH on MG adsorption on PVA nanofiber/ Fe₃O₄ nanoparticles

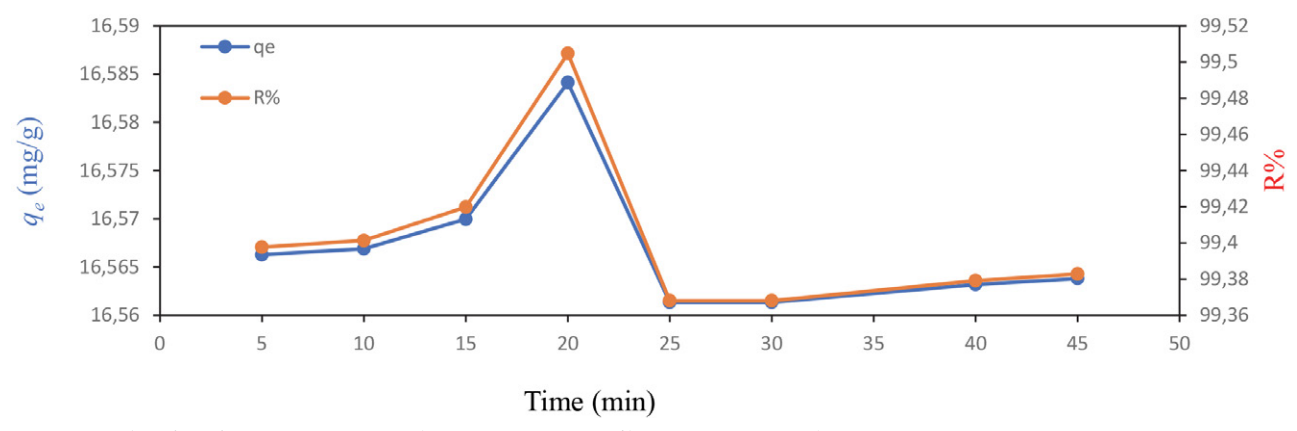


Figure 6: The effect of contact time on MG adsorption on PVA nanofiber/ Fe_3O_4 nanoparticles

sorption capacity dropped significantly at 25 min, became steady, and reached equilibrium at 45 min, when no more dye removal was noted. Therefore, 20 minutes was chosen as the maximum time for MG adsorption on PVA nanofiber/ Fe_3O_4 nanoparticles.

3. 3. Adsorption Kinetic Studies

Four kinetic models evaluate the process of adsorption and interpret the kinetic results to examine the kinetics of the mechanism of adsorption and select the optimum conditions of the operation. Pseudo-first-order, Pseudo-second-order equations, as well as, Elovich, and Intraparticle diffusion equations, were applied and represented as the following equations respectively. 46-49

3. 4. 1. Pseudo-first-order Model

$$log (q_e - q_t) = log q_e - \left(\frac{k_1}{2303}\right)t$$
 (3)

Where; q_e represents the adsorption capacity at equilibrium (mg/g), q_t represents the adsorption capacity at time (t) (mg/g), t means time (min), and k_1 is defined as the Lageragren rate constant of adsorption (min⁻¹). The q_e and k_1 values were determined from the intercept and the slope of the linear equation of $\ln(q_e - q_t)$ against t as shown in Figure 7, and found to be 0.018, and 0.005, respectively. Also, the correlation coefficient for this kinetic model which represents the R^2 value was 0.4147.

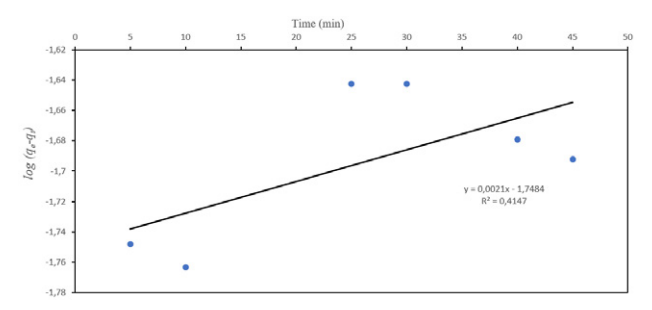


Figure 7: The pseudo-first-order kinetic model of adsorption of MG on PVA nanofiber/Fe₃O₄ nanoparticles

3. 4. 2. Pseudo-second-order Model

The pseudo-second-order model was then analyzed and given by the following equation:

$$\frac{t}{q_t} = \frac{1}{k_2 \ q_e^2} + \frac{1}{q_e}(t) \tag{4}$$

Here, k_2 is known as the rate constant of adsorption (g/mg min) for pseudo-second-order. Also, for this model, k_2 and q_e were found from the slope and the intercept of the linear plot of (t/q_t) against t, as shown in Figure 8, and found to be 9.12, and 16.55, respectively, while the R^2 value for pseudo-second-order was 1.00. These results refer to the fact that the MG dye adsorption onto the modified membrane follows the pseudo-second-order model. This denotes that the chemical adsorption (chemisorption) of Fe₃O₄ nanoparticles on PVA nanofiber is the rate determining step, and the total rate of the adsorption process of MG may be controlled by the chemical attraction between the adsorbent and adsorbate.⁵⁰

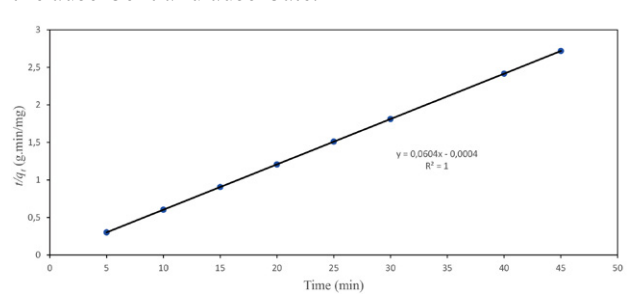


Figure 8: Pseudo-second-order kinetic model of adsorption of MG on PVA nanofiber/ Fe_3O_4 nanoparticles

3. 4. 2. Elovich Kinetic Model

Elovich kinetic model for the adsorption of MG was also studied, which usually can be expressed as in equation 5 and is dependent on the adsorption capacity q_t plot versus $\ln t$ (Figure 9). This equation was first used in studying the kinetics of chemical adsorption of gasses on the surface of solids, however, it has also been successfully applied

for the solute adsorption from liquid solutions.⁵¹

$$q_t = \frac{1}{\beta} \ln \left(\alpha \beta \right) + \frac{1}{\beta} \ln \left(t \right) \tag{5}$$

Where; the parameter a (mg/g min) is the initial sorption rate, and b (g/mg) is the extent of surface coverage and activation energy for chemical adsorption. The values are determined and displayed in Table 1.

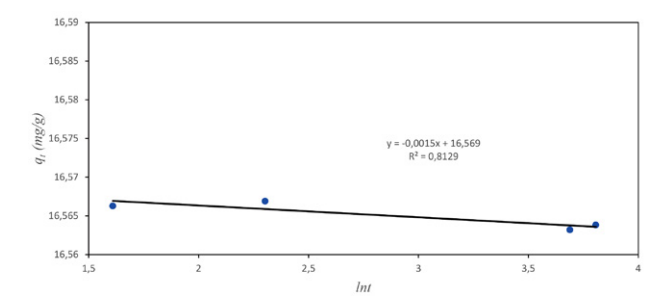


Figure 9: Elovich kinetic for the adsorption of MG on PVA nanofiber/ Fe_3O_4 nanoparticles

3. 4. 4. Intraparticle Diffusion

The intraparticle diffusion study is the most widely applied model for the identification mechanism in the process of adsorption, which is indicated as follows: ⁵²

$$q_t = K_{dif} t^{\frac{1}{2}} + B_L \tag{6}$$

Where; K_{dif} refers to the rate constant of the intraparticle diffusion (mg/g min), B_L is the intercept that points to the boundary layer thickness (mg/g). The q_t plot against $t^{1/2}$ is represented in Figure 10. The value of K_{dif} =0.0008 mg/g min, B_L =16.569 mg/g, while the R^2 values for the intraparticle diffusion is 0.866. The intercept value is directly proportional to the effect of the boundary layer, the higher the intercept value, the greater the effect the boundary layer has. By other means, the amount of the adsorbate on the boundary layer rises. ⁵³

3. 5. Effect of Initial Concentration of MG

Adsorption studies with different initial concentrations of 10 to 50 mg/L were carried out to calculate PVA

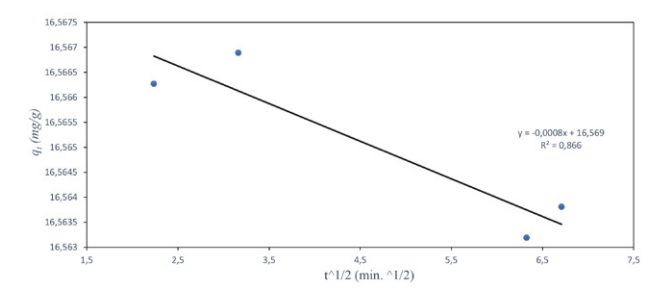


Figure 10: Intraparticle diffusion for the adsorption of MG on PVA nanofiber/Fe₃O₄ nanoparticles

nanofiber/Fe $_3$ O $_4$ nanoparticles adsorption capacity towards MG dye. The initial concentration of the dye plays an influential role in the adsorption capacity of the adsorbent. In this experiment, it was clear from the results that the adsorption capacity of the adsorbent increased with the increase of the initial concentration of dye from 10 to 50 mg/L. The relationship of the adsorption coefficient (q_e) against initial concentrations is given in Figure 11. Adsorption isotherms, on the other hand, are graphical representations that indicate the interaction of adsorbate molecules with adsorbent and provide information on proceeding with the adsorption system. 54

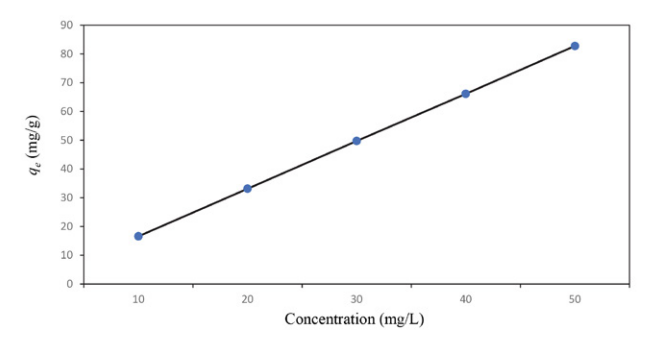


Figure 11: The effect of concentration on MG on PVA nanofiber/ Fe₃O₄ nanoparticles

Two well-known adsorption mathematical equations were used to interpret the equilibrium adsorption data. The first one was the Langmuir model, and the second was the Freundlich model, which is widely utilized to describe adsorption behavior. The Langmuir equation is:

Table 1: kinetic parameters of adsorption of MG on PVA nanofiber/Fe₃O₄ nanoparticles

Pseudo-first-order			Pseudo-second-order				
R^2 0.4147	<i>K</i> ₁ 0.005	q_e (calc.) 0.018	R^2 1	<i>K</i> ₂ 9.12	h 2500	q_e (calc.) 16.55	
Elovich model			Intra	Intraparticle diffusion			
R^2 0.8129	α 2.7182	β 666.6	R^2 0.866	K _{dif} 0.0008	B _L 16.569		

$$\frac{1}{q_e} = \left(\frac{1}{b \, q_m}\right) \frac{1}{C_e} + \frac{1}{q_m} \tag{7}$$

Here, q_e is the equilibrium adsorption capacity of the adsorbent (mg/g), b is the Langmuir adsorption constant (L/mg), q_m is the maximum capacity of the adsorbent

(mg/g) and C_e is the equilibrium MG concentration in solution (mg/L). Moreover, heterogeneous adsorption systems can be described by the linear form of the Freundlich equation, which is represented as the following equation:

$$lnq_e = ln \, ln \, k_f + \frac{1}{n} ln \, C_e \tag{8}$$

Table 2: Adsorption isotherm constants for PVA nanofiber/Fe₃O₄ nanoparticles

Langmuir			Freundlich		
R^2 0.9771	b (L/mg) 3.39	q _m (mg/g) 128.205	R^2 0.9692	$k_f(\text{mg/g})$ 169.76	n 1.3460

Table 3: Maximum adsorption capacity (q_m) of MG dye onto different reported adsorbents.

Adsorbent	q_m (mg/g)	Adsorbent dose/ dye volume (g/ml)	Reference
Alg-Fe ₃ O ₄ NPs	47.84	0.03 g/ 50 ml	6
PVA NF/Fe ₃ O ₄ NPs	128.205	0.003g/ 5 ml	This study
Coal fly ash / CoFe ₂ O ₄	90.9	0.6 g/ 150 ml	58
Wood apple shell	35.84	0.15 g/ 1000 ml	59
Zein/Graphene oxide	86.95	0.01 g/ 10 ml	60
CNF-Ag NPs	142.8	0.01 g/ 20 ml	61
Au-NP-AC	140.85	0.015 g/ 50 ml	62
Fe-Zn-PVA NCs	92.59	0.02 g/ 50 ml	63
Fe ₃ O ₄ / Sawdust Carbon	41.66	0.2–1 g/100ml	64

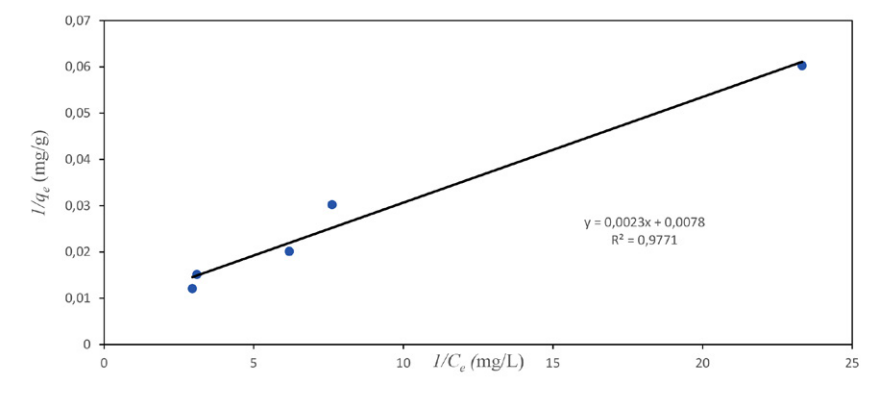


Figure 12: (a) Langmuir plot indicates the linear change of $1/q_e$ with $1/C_e$

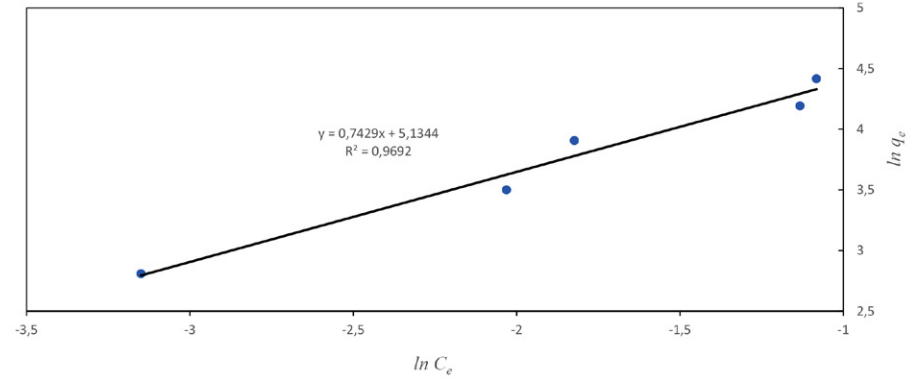


Figure 12: (b) Freundlich plot indicating the linear change of $\ln q_e$ on $\ln C_e$.

Where; K_f is the Freundlich constant (mg/g), n is the heterogeneity factor, and q_e and C_e are described above. ^{55,56} The values of q_m and b were acquired from the intercept and slope of the linear plot of $1/q_e$ against $1/C_e$ (Figure 12: a), while k_f and n values were calculated from the intercept and slope of the linear plot of $\ln q_e$ versus $\ln C_e$ (Figure 12: b), respectively. Table 2 lists the constants and coefficients of Langmuir and Freundlich adsorption isotherms. The results show that the data of equilibrium adsorption isotherms fit well in both Langmuir and Freundlich linear equations. The R² value in Langmuir was 0.9771, and in Freundlich was 0.9692. These two values are close, but they are more fitted to Langmuir, and according to the Langmuir equation, the MG molecules adsorption happens on the surface of the homogeneous adsorbent as monolayer coverage.⁵⁷ According to the Langmuir equation, the maximum adsorption capacity of PVA nanofiber/ Fe₃O₄ nanoparticle towards MG dye was calculated to be 128.205 mg/g, which indicates a higher capacity than the previously stated adsorbents (Table 3). Moreover, the n value of 1.3460 means that the adsorption of MG on PVA nanofiber/Fe₃O₄ nanoparticle is a favorable process.

4. Conclusions

To conclude, the significance of this study is to composite PVA nanofiber with iron oxide nanoparticles by simple hot water treatment, which is a simple and efficient technique. This study proves that the PVA nanofiber/ Fe₃O₄ nanoparticles membrane is very efficient, and the preparation process is highly economical. This newly synthesized material can be used as an adsorbent to remove MG dye from contaminated water. The study shows that the quantity of the adsorbed dye depends on the pH, adsorbent contact time, and initial dye concentration. Furthermore, the removal of dye is rapid, and the maximum removal is at 20 minutes then dropped to be steady and reach equilibrium. The adsorption rate follows pseudo-second-order kinetics and the Langmuir model of adsorption isotherm. Thus, the main advantage of PVA nanofiber/ Fe₃O₄ nanoparticles is that the maximum adsorption capacity is in progress compared with other studies and the adsorption rate is fast. Also, the method of preparation is very appropriate and practical. Our results showed that utilizing the HWT to integrate PVA nanofiber with Fe₃O₄ nanoparticles modified and improved the crosslinking of nanofiber. Also, the enhanced removal percentage of MG dye is promising for an effective, low-cost, eco-friendly alternative method for the removal of MG dye from several industries wastewater.

Acknowledgments

The authors thank the UoD PEER laboratory for supporting this work at the University of Duhok.

Conflicts of Interest

The authors declare that there are no competing financial interests.

5. Reference

- 1 J. O. Tijani, O. O. Fatoba, G. Madzivire and L. F. Petrik, *Water, Air, Soil Pollut.*, **2014**, 225, 2102.
 - DOI:10.1007/s11270-014-2102-y
- 2 H. Zangeneh, A. A. L. Zinatizadeh, M. Habibi, M. Akia and M. Hasnain Isa, J. Ind. Eng. Chem., 2015, 26, 1–36. DOI:10.1016/j.jiec.2014.10.043
- 3 H. Sun, J. Jiang, Y. Xiao and J. Du, ACS Appl. Mater. Interfaces, 2018, 10, 713–722. DOI:10.1021/acsami.7b15242
- 4 B. M. Thamer, A. Aldalbahi, M. Moydeen A, M. Rahaman and M. H. El-Newehy, *Polymers (Basel).*, **2020**, *13*, 20. **DOI:**10.3390/polym13010020
- 5 W. Zhang, L. Wang, E. Mäkilä, S. Willför and C. Xu, *Ind. Crops Prod.*, **2022**, *177*, 114513. **DOI**:10.1016/j.indcrop.2021.114513
- 6 A. Mohammadi, H. Daemi and M. Barikani, *Int. J. Biol. Macromol.*, **2014**, *69*, 447–455.

DOI:10.1016/j.ijbiomac.2014.05.042

- R. K. Gautam, V. Rawat, S. Banerjee, M. A. Sanroman, S. Soni,
 S. K. Singh and M. C. Chattopadhyaya, *J. Mol. Liq.*, 2015, 212,
 227–236. DOI:10.1016/j.molliq.2015.09.006
- 8 P. Arabkhani and A. Asfaram, *J. Hazard. Mater.*, **2020**, *384*, 121394. **DOI:**10.1016/j.jhazmat.2019.121394
- N. Y. Donkadokula, A. K. Kola, I. Naz and D. Saroj, Rev. Environ. Sci. Bio/Technology, 2020, 19, 543–560.
 DOI:10.1007/s11157-020-09543-z
- 10 L. Qiu, Y. Peng, B. Liu, B. Lin, Y. Peng, M. J. Malik and F. Yan, Appl. Catal. A Gen., 2012, 413–414, 230–237.
 DOI:10.1016/j.apcata.2011.11.013
- 11 G. Yang, N. Zhang, J. Yang, Q. Fu, Y. Wang, D. Wang, L. Tang, J. Xia, X. Liu, X. Li, Q. Yang, Y. Liu, Q. Wang and B.-J. Ni, Water Res., 2020, 169, 115249. DOI:10.1016/j.watres.2019.115249
- B. Zaarour, L. Zhu and X. Jin, ChemistrySelect, 2020, 5, 1335– 1348. DOI:10.1002/slct.201903981
- 13 B. Zaarour and M. F. Alhinnawi, *J. Ind. Text.*, **2022**, *51*, 1S–35S. **DOI:**10.1177/15280837221083031
- 14 B. Zaarour, L. Zhu, C. Huang and X. Jin, *Polym. Adv. Technol.*, 2020, 31, 1449–1462. DOI:10.1002/pat.4876
- 15 M. El-Kammah, E. Elkhatib, S. Gouveia, C. Cameselle and E. Aboukila, *Sustain. Chem. Pharm.*, **2022**, 29, 100753. **DOI:**10.1016/j.scp.2022.100753
- O. A. Shabaan, H. S. Jahin and G. G. Mohamed, *Arab. J. Chem.*,
 2020, 13, 4797–4810. DOI:10.1016/j.arabjc.2020.01.010
- 17 N. Torasso, A. Vergara-Rubio, P. Rivas-Rojas, C. Huck-Iriart, A. Larrañaga, A. Fernández-Cirelli, S. Cerveny and S. Goyanes, *J. Environ. Chem. Eng.*, 2021, 9, 104664. DOI:10.1016/j.jece.2020.104664
- 18 S. Xiao, M. Shen, R. Guo, S. Wang and X. Shi, *J. Phys. Chem. C*, **2009**, *113*, 18062–18068. **DOI**:10.1021/jp905542g
- 19 F. He and D. Zhao, Environ. Sci. Technol., 2005, 39, 3314-20.

- **DOI:**10.1021/es048743y
- 20 X. Wang, M. Zhu, H. Liu, J. Ma and F. Li, *Sci. Total Environ.*, 2013, 449, 157–67. DOI:10.1016/j.scitotenv.2013.01.008
- 21 L. M. Kustov, E. D. Finashina, E. V. Shuvalova, O. P. Tkachenko and O. A. Kirichenko, *Environ. Int.*, **2011**, *37*, 1044–1052. **DOI:**10.1016/j.envint.2011.05.003
- 22 T. Shahwan, M. Anjass and R. Naser, *J. Mater. Environ. Sci.*, 2021, vol. 12.
- 23 J. Liu, N. Wang, H. Zhang and J. Baeyens, J. Environ. Manage., 2019, 238, 473–483. DOI:10.1016/j.jenvman.2019.03.009
- 24 D. Talbot, J. Queiros Campos, B. L. Checa-Fernandez, J. A. Marins, C. Lomenech, C. Hurel, G. D. Godeau, M. Raboisson-Michel, G. Verger-Dubois, L. Obeid, P. Kuzhir and A. Bee, ACS Omega, 2021, 6, 19086–19098.
 DOI:10.1021/acsomega.1c02401
- 25 V. K. Yadav, D. Ali, S. H. Khan, G. Gnanamoorthy, N. Choudhary, K. K. Yadav, V. N. Thai, S. A. Hussain and S. Manhrdas, Nanomaterials, 2020, 10, 1551. DOI:10.3390/nano10081551
- 26 J. G. Darab, A. B. Amonette, D. S. D. Burke, R. D. Orr, S. M. Ponder, B. Schrick, T. E. Mallouk, W. W. Lukens, D. L. Caulder and D. K. Shuh, *Chem. Mater.*, 2007, 19, 5703–5713. DOI:10.1021/cm0607379
- 27 N. Rajput, Int. J. Adv. Eng. Technol., 2015, 7, 1806–1811.
- 28 N. S. Saadi, L. B. Hassan and T. Karabacak, *Sci. Rep.*, **2017**, *7*, 7158. **DOI:**10.1038/s41598-017-07783-8
- 29 A. Rianjanu, A. Kusumaatmaja, E. A. Suyono and K. Tryana, Heliyon, 2018, 4, 2405-8440. DOI:10.1016/j.heliyon.2018.e00592
- 30 T.-M. Huang, F. Pang, I.-F. Hsieh and M. Cakmak, *Synth. Met.*, **2016**, *221*, 309–318. **DOI:**10.1088/1757-899X/429/1/012019
- 31 N. S. A. Halim, M. D. H. Wirzal, M. R. Bilad, A. R. M. Yusoff, N. A. H. M. Nordin, Z. A. Putra and J. Jaafar, *IOP Conf. Ser. Mater. Sci. Eng.*, 2018, 429, 012019. DOI:10.1016/j.memsci.2012.12.037
- 32 L. Huang, S. S. Manickam and J. R. McCutcheon, *J. Memb. Sci.*, 2013, 436, 213–220. DOI:10.1016/j.memsci.2016.03.062
- 33 C. Liu, X. Li, T. Liu, Z. Liu, N. Li, Y. Zhang, C. Xiao and X. Feng, *J. Memb. Sci.*, **2016**, *512*, 1–12. **DOI:**10.1016/j.synthmet.2016.09.009
- 34 Q. Ren, C. Kong, Z. Chen, J. Zhou, W. Li, D. Li, Z. Cui, Y. Xue and Y. Lu, *Microchem. J.*, 2021, 164, 106059.
 DOI:10.1016/j.microc.2021.106059
- 35 W. Qu, T. Yuan, G. Yin, S. Xu, Q. Zhang and H. Su, *Fuel*, **2019**, 249, 45–53. **DOI:**10.1016/j.fuel.2019.03.058
- S. Mohanraj, S. Kodhaiyolii, M. Rengasamy and V. Pugalenthi, *Appl. Biochem. Biotechnol.*, **2014**, *173*, 318–331.
 DOI:10.1007/s12010-014-0843-0
- 37 J. A. A. Abdullah, L. Salah Eddine, B. Abderrhmane, M. Alonso-González, A. Guerrero and A. Romero, Sustain. Chem. Pharm., 2020, 17, 100280. DOI:10.1016/j.scp.2020.100280
- M. Srivastava, J. Singh, M. Yashpal, D. K. Gupta, R. K. Mishra,
 S. Tripathi and A. K. Ojha, *Carbohydr. Polym.*, 2012, 89, 821–829. DOI:10.1016/j.carbpol.2012.04.016
- 39 A. Moharana, D. Kumar and A. Kumar, *J. Phys. Conf. Ser.*, **2020**, *1531*, 012113. **DOI**:10.1088/1742-6596/1531/1/012113
- 40 S. Kayal and R. V. Ramanujan, *Mater. Sci. Eng. C*, **2010**, *30*, 484–490. **DOI**:10.1016/j.msec.2010.01.006

- 41 P. Bahmani, A. Maleki, H. Daraei, R. Rezaee, M. Khamforoush, S. Dehestani Athar, F. Gharibi, A. H. Ziaee and G. McKay, *Environ. Sci. Pollut. Res.*, 2019, 26, 21993–22009. DOI:10.1007/s11356-019-05228-5
- 42 S. Ju, T.-Y. Cai, H.-S. Lu and C.-D. Gong, *J. Am. Chem. Soc.*,
 2012, 134, 13780–13786.
 DOI:10.1021/ja305167h
- 43 E. Bulut, M. Özacar and İ. A. Şengil, *Microporous Mesoporous Mater.*, 2008, 115, 234–246.
 DOI:10.1016/j.micromeso.2008.01.039
- 44 G. Crini, H. Peindy, F. Gimbert and C. Robert, Sep. Purif. Technol., 2007, 53, 97–110. DOI:10.1016/j.seppur.2006.06.018
- 45 S. Arellano-Cárdenas, S. López-Cortez, M. Cornejo-Mazón and J. C. Mares-Gutiérrez, *Appl. Surf. Sci.*, 2013, 280, 74–78. DOI:10.1016/j.apsusc.2013.04.097
- 46 Uma, S. Banerjee and Y. C. Sharma, *J. Ind. Eng. Chem.*, **2013**, *19*, 1099–1105. **DOI**:10.1016/j.jiec.2012.11.030
- 47 B. H. Hameed and M. I. El-Khaiary, *J. Hazard. Mater.*, **2008**, 153, 701–708. **DOI**:10.1016/j.jhazmat.2007.09.019
- 48 F. Othman, M. S. Sadeghian, F. Ebrahimi and M. Heydari, *Int. Proc. Chem. Biol. Environ. Eng.*, **2013**, *51*, 6. **DOI**:10.7763/ipcbee
- 49 T. Shean, Y. Choong, K. L. Lau, M. Abdullah and S. N. A. MD Jamil, *Materials (Basel).*, 2019, 12, 1–17.
 DOI:10.3390/ma12111734
- 50 H. Sun, L. Cao and L. Lu, Nano Res., 2011, 4, 550–562. DOI:10.1007/s12274-011-0111-3
- 51 C. Gerente, V. K. C. Lee, P. Le Cloirec and G. McKay, Crit. Rev. Environ. Sci. Technol., 2007, 37, 41–127. DOI:10.1080/10643380600729089
- 52 G. Vijayakumar, C. K. Yoo, K. G. P. Elango and M. Dharmendirakumar, *Clean Soil, Air, Water*, **2010**, *38*, 202–209. **DOI:**10.1002/clen.200900125
- 53 T. S. Najim and S. A. Yassin, *E-Journal Chem.*, **2009**, *6*, S153–S158. **DOI**:10.1155/2009/804256
- 54 C. Ng, J. N. Losso, W. E. Marshall and R. M. Rao, *Bioresour. Technol.*, **2002**, 85, 131–5.
 DOI:10.1016/S0960-8524(02)00093-7
- 55 E. Lorencgrabowska and G. Gryglewicz, *Dye. Pigment.*, **2007**, 74, 34–40. **DOI**:10.1016/j.dyepig.2006.01.027
- 56 H. A. Ahmed, P. H. Saleem, S. A. Yasin and I. A. Saeed, in Journal of Physics: Conference Series, 2021,1853, 012006. DOI:10.1088/1742-6596/1853/1/012006
- 57 X. Guo and J. Wang, *J. Mol. Liq.*, **2019**, *296*, 111850. **DOI:**10.1016/j.molliq.2019.111850
- 58 M. Zhang, Y. Mao, W. Wang, S. Yang, Z. Song and X. Zhao, *RSC Adv.*, **2016**, *6*, 93564–93574. **DOI**:10.1039/C6RA08939A
- 59 A. S. Sartape, A. M. Mandhare, V. V. Jadhav, P. D. Raut, M. A. Anuse and S. S. Kolekar, *Arab. J. Chem.*, **2017**, *10*, S3229–S3238. **DOI:**10.1016/j.arabjc.2013.12.019
- 60 A. S. Keshtiban, S. M. Seyedahmadian, B. Habibi and K. Farhadi, *Prog. Color. Color. Coatings*, **2021**, *14*, 55–65. **DOI**: 10.30509/pccc.2021.81679
- 61 N. Chinthalapudi, V. V. D. Kommaraju, M. K. Kannan, C. B. Nalluri and S. Varanasi, *Carbohydr. Polym. Technol. Appl.*, **2021**, *2*, 100098. **DOI:**10.1016/j.carpta.2021.100098

- 62 M. Roosta, M. Ghaedi, N. Shokri, A. Daneshfar, R. Sahraei and A. Asghari, *Spectrochim. Acta. A. Mol. Biomol. Spectrosc.*, **2014**, *118*, 55–65. **DOI:**10.1016/j.saa.2013.08.082
- 63 M. Saad, H. Tahir, S. Mustafa, O. A. Attala, W. A. El-Saoud, K.
- A. Attia, W. M. Filfilan and J. Zeb, Nanomaterials, 2023, 13, 1747. DOI:10.3390/nano13111747
- 64 Z. Bonyadi, F. S. Khatibi and F. Alipour, Appl. Water Sci., 2022, 12, 221. DOI:10.1007/s13201-022-01745-w

Povzetek

Študija opisuje uporabo hlapov topil za obdelavo in povečano zamreženje PVA nanovlaken. S preprosto tehniko vroče vode so bili sintetizirani nanodelci Fe₃O₄ v kompozitu z nanovlakni. Študija se osredotoča na uporabo modificiranih PVA nanovlaken za odstranjevanje malahitno zelene (MG) iz vode pri različnih pH, kontaktnih časih in začetnih koncentracijah barvila. Površinska morfologija nanovlaken je bila določena s tehnikami SEM, FTIR in XRD. SEM je pokazal, da se je zamreženje povečalo, Fe₃O₄ nanodelci pa so se pojavili kot aglomerati na površini nanovlaken. Odstotek odstranjevanja pri optimalnem pH in kontaktnem času je bil 99,76 % oziroma 99,5 %. Nato smo proučevali kinetiko z linearnimi modeli psevdo-prvega reda, psevdo-drugega reda, Elovicheve enačbe in modela notranje difuzije. Rezultati so pokazali, da kinetika adsorpcije sledi psevdo-drugemu redu. Poleg tega smo adsorpcijsko izotermo potrjevali z uporabo Langmuirjeve in Freundlichove enačbe. Langmuirjeva enačba je najbolje opisala adsorpcijo z vrednostjo R² 0,9771, največja odstranitev pa je bila 128,205 mg/g. Posledično so molekule barvila MG prekrile nanovlakna PVA/nanodelci Fe₃O₄ v enoslojni in homogeni plasti. Rezultati študije so pomembni za čiščenje odpadne vode v industriji, saj zagotavljajo možno rešitev za odstranitev barvila MG iz odpadne vode v tekstilni, papirni, kozmetični, živilski in ribogojni industriji.



Except when otherwise noted, articles in this journal are published under the terms and conditions of the Creative Commons Attribution 4.0 International License